Nested Fermi Surface and Electronic Instability in $Ca_3Ru_2O_7$

F. Baumberger,[1] N. J. C. Ingle,[1,2] N. Kikugawa,[3] M. A. Hossain,[2] W. Meevasana,[1] R. S. Perry,[4] K. M. Shen,[1,2] D. H. Lu,[1] A. Damascelli,[2] A. Rost,[3] A. P. Mackenzie,[3] Z. Hussain,[5] and Z.-X. Shen[1]

[1]*Departments of Applied Physics and Physics, and Stanford Synchrotron Radiation Laboratory, Stanford University, Stanford, California 94305, USA*

[2]*Department of Physics and Astronomy, University of British Columbia, Vancouver, British Columbia V6T 1Z4, Canada*

[3]*School of Physics and Astronomy, Scottish Universities Physics Alliance, University of St. Andrews, St. Andrews, Fife KY16 9SS, Scotland*

[4]*Department of Physics, Kyoto University, Kyoto 606-8501, Japan*

[5]*Advanced Light Source, Lawrence Berkeley National Laboratory, Berkeley, California 94720, USA*

(Received 15 July 2005; published 17 March 2006)

High-resolution angular resolved photoemission data reveal well-defined quasiparticle bands of unusually low weight, emerging in line with the metallic phase of $Ca_3Ru_2O_7$ below ~30 K. At the bulk structural phase transition temperature of 48 K, we find clear evidence for an electronic instability, gapping large parts of the underlying Fermi surface that appears to be nested. Metallic pockets are found to survive in the small, non-nested sections, constituting a low-temperature Fermi surface with 2 orders of magnitude smaller volume than in all other metallic ruthenates. The Fermi velocities and volumes of these pockets are in agreement with the results of complementary quantum oscillation measurements on the same crystal batches.

DOI: 10.1103/PhysRevLett.96.107601 PACS numbers: 71.18.+y, 71.45.Lr, 79.60.−i

The characterization and description of novel phases found in transition metal oxides (TMOs) has stimulated progress in condensed matter physics over the last decades [1]. The itinerant electron system of the perovskite ruthenium oxides provides a prime opportunity to study such complex ground states and phase transitions or competition in TMOs starting from a quasiparticle (QP) band structure picture [2]. Ruthenates can be grown with extremely high purity, which has allowed detailed studies of the Fermi surface (FS) topology through the detection of quantum oscillations (QOs) [3,4], and Sr_2RuO_4 has served as a benchmark system for the potential of angular resolved photoemission (ARPES) to derive quantitative information on band dispersion and QP scattering rates [5,6]. Although these studies yielded fully consistent results, it should be noted that ARPES probes a larger energy scale and can reveal information that is complimentary to low-temperature transport and thermodynamic measurements.

While all Sr-based ruthenates of the Ruddlesden-Popper series $(Sr, Ca)_{n+1}Ru_nO_{3n+1}$ are metallic at low temperature, the situation becomes more ambiguous upon substitution of Sr with the isovalent but smaller Ca ion. This causes structural distortions leading to a rotation and tilting of the RuO_6 octahedra, which in turn reduces hopping matrix elements and thus emphasizes correlation effects [7,8]. The subject of this study, $Ca_3Ru_2O_7$, has been reported to be ''semimetallic,'' with two phase transitions, a Néel transition at 56 K and a structural phase transition at 48 K [9], where the *in-plane* resistivity increases by about 30%. At lower temperatures the resistivity is metallic, but very large [10–12].

In this Letter, we report the growth of crystals with an order of magnitude lower residual resistivity than previously achieved, and high-resolution ARPES and QO measurements on them. We find an extremely small QP residue Z (fraction of spectral weight in the coherent quasiparticle excitation), extended parallel Fermi surface sections, and a momentum dependent gap, opening at the bulk phase transition temperature. Comparison of Fermi volumes and velocities from the two techniques establishes the ground state of $Ca_3Ru_2O_7$ as a low carrier density metal. Together, the data indicate that the unusual ground state results from a Peierls-like electronic instability, gapping away large parts of the Fermi surface.

Photoemission experiments were performed with a Scienta SES 2002 spectrometer, using He $I\alpha$ radiation (21.22 eV) from a microwave driven monochromatized discharge lamp (Gammadata VUV5000). The differential pumping of the He leakage from the plasma chamber has been optimized to provide a partial pressure in the measurement chamber near the sensitivity limit of UHV ion gauges, without restricting the large solid angle of ≈10° collected by the refocusing toroidal monochromator. Energy and angular resolutions were set to 7.5 meV/ ± 0.15° for all measurements. Single crystals of $Ca_3Ru_2O_7$ with lowest residual in-plane resistivity of 40 $\mu\Omega$ cm were grown by a floating zone method [12], oriented by Laue diffraction and cleaved *in situ* at a pressure below 5×10^{-11} torr along the *ab* plane. Samples cleaved at 10 and 60 K yielded consistent results and the low-energy spectra showed minimal changes over the time span of a typical experimental run of 24 h. Magnetoresistance and the Hall effect were studied between 50 mK and 1 K in a dilution refrigerator/15 T magnet.

Full details of our QO and magnetotransport measurements will be published elsewhere, but to form a basis for

comparison with the ARPES results we summarize them here. The Fermi surface consists of tiny, quasi-two-dimensional pockets of electrons and holes, typical areas 0.3% of that of the Brillouin zone (BZ). The measured quasiparticle effective masses correspond to Fermi velocities of approximately 5×10^4 m/s. The masses account, within experimental error, for the small electronic specific heat of 2.8 mJ/mol K^2, which we measured on the same crystals, so we are confident that the QOs are probing the entire Fermi surface.

In Fig. 1, we compare the ARPES spectra of $Ca_3Ru_2O_7$ and $Sr_3Ru_2O_7$ over a large energy range. The isoelectronic nature upon substitution of Sr with Ca is clearly reflected in the spectra which show similar energies and dispersive behavior of the main valence band peaks. Despite this gross similarity of the lower valence states, there is a striking difference in the spectral function near the Fermi level (E_F). While $Sr_3Ru_2O_7$ shows intense quasiparticle peaks and multiple bands crossing the Fermi level, the spectral weight in $Ca_3Ru_2O_7$ is dramatically suppressed below $\sim$150 meV and only a weak tail extends towards E_F [Fig. 1(c)]. For the rest of the Letter, we will focus on this tail, which reflects the lowest lying excitations responsible for the transport and thermodynamic properties. The high resolution and stability of our spectrometer has allowed us for the first time to observe well-defined quasiparticle bands, emerging on this faint tail below a temperature of $\approx$ 30 K, in line with the onset of coherent metallic transport in the *ab* plane [10,12]. These states exhibit an extremely low QP residue Z, over an order of magnitude lower than in $Sr_3Ru_2O_7$, indicative of strongly enhanced interactions, but remain sharply defined in energy. From fits to empirical spectral functions [see Fig. 1(d)], we estimate an intrinsic lifetime broadening $\Sigma_I \approx 5$ meV at binding energies around 15–20 meV, comparable to the value found for the intense quasiparticle peaks in the moderately correlated Fermi liquid compound Sr_2RuO_4 [5]. For a Fermi liquid with momentum independent self-energy, the QP spectral weight depends only on the mass enhancement and therefore on the scattering rate. The observation of sharp QPs at energies >15 meV with small Z thus points to strongly momentum and possibly orbital dependent interactions [13].

The momentum distribution of the spectral weight near E_F is shown in Figs. 2(a) and 2(b). These maps are often casually identified with the Fermi surface. However, the present case requires a more careful interpretation. Integrating the spectral weight over a typical energy range of $E_F \pm 12$ meV results in two dominant structures, as summarized in Fig. 2(c): a "*large square*" contour with rounded corners, connecting the M points of the reduced orthorhombic BZ, and a smaller, more intense square composed of four broad triangular features. The identification of these contours as Fermi surface sheets would conflict with the QO data, which indicate extremely small

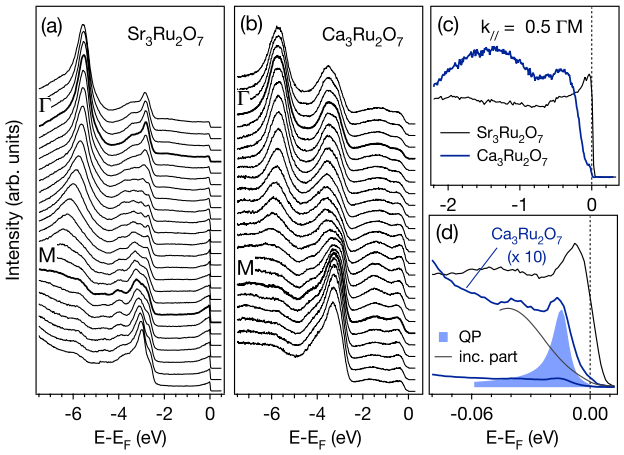

FIG. 1 (color online). (a),(b) Valence band spectra of $Sr_3Ru_2O_7$ and $Ca_3Ru_2O_7$ taken with equal momentum steps along ΓM ($h\nu = 21.2$ eV, $T = 10$ K). In (c) and (d), spectra of the two compounds have been normalized to the total spectral weight of the valence band (integrated from 0 to -7 eV) and are compared on two different energy scales. A fit of the low-energy weight assuming a FL-like QP on a rising incoherent part, indicates a self-energy $\Sigma_I \approx 5$ meV at $E - E_F \approx 15$ meV.

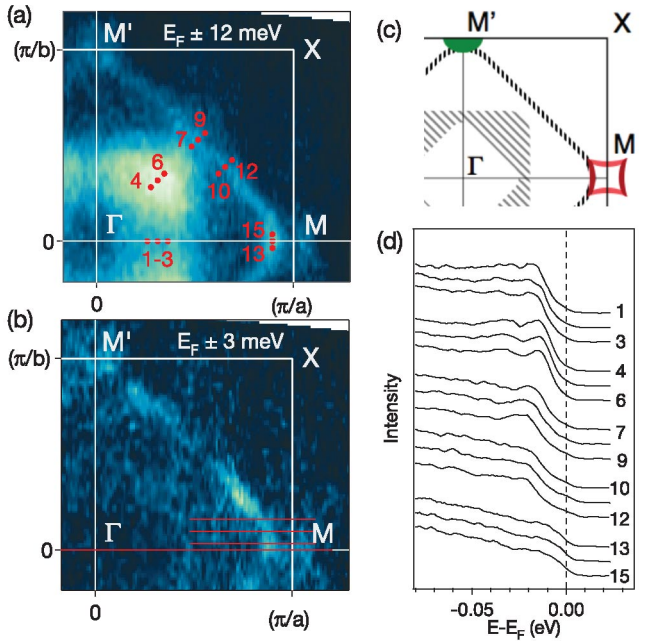

FIG. 2 (color). (a),(b) Momentum distribution of the lowest lying spectral weight in $Ca_3Ru_2O_7$ at $T = 9$ K. The two different energy windows correspond to effective resolutions of 25 and 10 meV, respectively. Red lines in (b) indicate momentum space locations of the dispersion plots in Fig. 3. (c) Schematic of the dominant features in the low-energy excitations. The small Fermi arc near the M point is backfolded by the proposed nesting vector to connect to a closed Fermi surface contour (see text). (d) Selected spectra, extracted from the data set of (a) and (b) demonstrating different gap sizes for various points in the BZ. Metallic states are found only in the vicinity of the M points.

carrier pockets with an average volume of only 0.3% of the BZ. It is important to elucidate the origin of the apparent inconsistency, because large FS sheets are expected from band structure calculations [14] and were observed in the isovalent $Sr_3Ru_2O_7$ in density functional calculations [15], ARPES [16,17], and de Haas–van Alphen data [4].

In Fig. 2(b), the spectral weight is integrated over a narrower energy range of ± 3 meV. Clearly, this suppresses the intense inner square contour, indicating that the constituting states are gapped and do not contribute to the Fermi surface. Extracting energy distribution curves (EDCs) at selected momentum points from the same data set confirms this finding. The spectra at points 1–3 and 4–6, marked in Fig. 2(a), show weakly dispersing, faint QP peaks and a clear leading edge that is gapped by 5–9 meV [Fig. 2(d)]. Next, we focus on the large square contour. Two sets of spectra, crossing it (7–9, 10–12) show tails extending up to E_F but a distinct leading edge with midpoints (LEM) clearly below the Fermi level. Metallic states with a LEM at the chemical potential are found only in the rounded edges of the large square, near the M points. Summarizing the data of Fig. 2, we find a peak in the zero-frequency momentum distribution (bright spot in the Fermi surface map), coexisting with a leading edge gap. This behavior is characteristic for systems where an electronic instability such as a charge density wave or the formation of Cooper pairs opens a gap in the single particle excitation spectrum. Assuming a particle-hole symmetric but gapped band, the remnant intensity in the photoemission Fermi surface map can be identified with the underlying band structure *before* the instability gapped away most of the FS [18]. The diamond shape seen in Fig. 2(b) suggests that the FS of $Ca_3Ru_2O_7$ is composed of quasi-1D $d_{xz,yz}$ orbitals, as detailed in Ref. [12]. Strikingly, the detected underlying FS contour exhibits extended parallel sections and is almost perfectly nested with the vector $(\pi/a, \pi/b)$ corresponding to a real space periodicity of two Ru-Ru nearest neighbor distances. Based on this finding, we postulate the formation of a commensurate density wave below 48 K. This idea is fully consistent with the temperature dependence of the gap, the QO data, and the low electronic specific heat as will be shown later.

The postulate of a density wave in $Ca_3Ru_2O_7$, introducing the new periodicity of $(\pi/a, \pi/b)$, is further supported by the details of the quasiparticle dispersion, shown in Fig. 3. The dispersion of the metallic states in the rounded corners of the underlying FS is traced in Fig. 3(a) by white dots, obtained from Lorentzian fits of the momentum distribution curves (MDCs). The group velocity of ≈ 0.26 eV Å for this band is in good agreement with the estimate of 5×10^4 m/s (0.33 eV Å) from the QOs. The evolution of the dispersion upon approaching the nested sections of the underlying FS is shown in Figs. 3(c)–3(e). Moving away from the high symmetry line by as little as $0.09\pi/b$ [Fig. 3(d)], the QP band starts to bend back and a

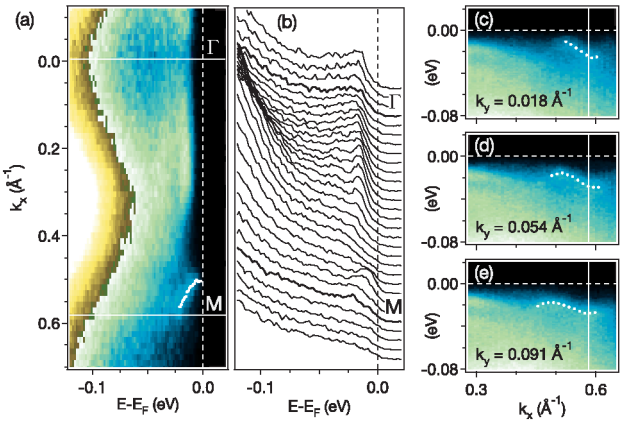

FIG. 3 (color). (a),(b) Dispersion of QP states along ΓM displayed as false color plot or stack of equally spaced EDCs, respectively. A metallic band is found near the M point. White dots indicate the peak positions found from Lorentzian fits to MDCs. (c)–(e) are taken along the momentum space lines indicated in Fig. 2(b) and show in detail how the bands bend back and a gap opens as the nested part of the underlying FS is approached. White dots mark the peak positions in EDCs.

gap of a few meV opens. This raises the intriguing question of how the Fermi level crossing around $0.88(\pi/a)$, seen in Fig. 3(a), connects to a closed FS contour. Folding the rounded corner of the large square by the newly imposed periodicity corresponding to the nesting vector of $(\pi/a, \pi/b)$, we would expect a roughly square electron pocket centered at M with slightly concave edges, as sketched in Fig. 2(c). The volume of such a pocket can be estimated as $(0.12\pi/a)^2 \sim 0.36\% A_{\mathrm{BZ}}$, assuming a simple square shape, in good agreement with the average FS-sheet volume deduced from the QOs. The apparent absence of the folded bands in the FS map and dispersion plots does not disprove this model, since the intensity of folded bands in ARPES is proportional to the coupling responsible for the folding [18]. Taking the energy gap (~ 5 meV) as a measure of this coupling, and comparing it to typical band gap sizes (~ 0.5 eV), we expect a suppression of the folded bands to intensities clearly below a level detectable by ARPES. Additional metallic states are found near M', but the band topology is less clear, in part because of the smaller BZ-dimension along b, which moves the zone boundary closer to the edge of the large square contour.

In Fig. 4, we show the temperature and momentum dependence of the gap. The direct comparison of spectra taken above and below the 48 K phase transition temperature along the high symmetry line ΓM [Fig. 4(a)] clearly demonstrates a significant momentum dependence in the low-temperature phase and confirms that the states in the corners of the low-energy square contour remain metallic: the highlighted spectra at point 1 show identical leading edge midpoints, which coincide within the experimental error with the Fermi level. The evolution of the low-energy spectral weight with temperature is shown in Fig. 4(b) for

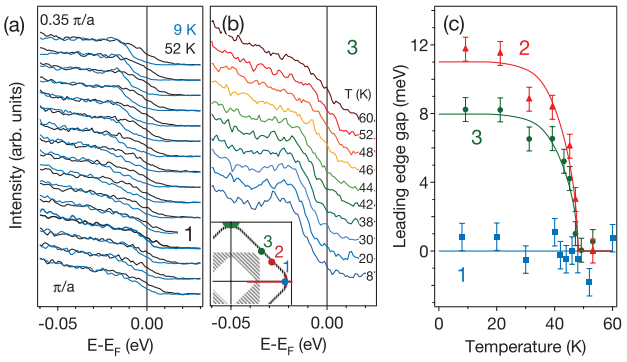

FIG. 4 (color). Temperature and momentum dependence of the gap. (a) shows spectra taken at 9 and 52 K along the red line depicted in the BZ inset. (b) Temperature series of spectra at point 3. (c) Evolution of the leading edge gap with temperature for momentum space points 1–3 with $(k_x, k_y) = (0.88\frac{\pi}{a}, 0)$, $(0.69\frac{\pi}{a}, 0.34\frac{\pi}{b})$, and $(0.5\frac{\pi}{a}, 0.5\frac{\pi}{b})$, respectively.

point 3 marked in the BZ inset. The spectral line shape does not change significantly at the Néel transition temperature of 56 K, and only a minor redistribution of weight occurs at 48 K. This is consistent with the weak perturbation, expected from a symmetry breaking ordering with low phase transition temperature and small gap. More pronounced changes of the spectral function are observed below 35 K, where sharply defined, faint QP peaks emerge. Notably this coincides with the onset of metallic transport, roughly 10 K below the structural phase transition temperature [12], rather than with the transition temperature itself.

Leading edge gaps Δ_{LE} were obtained from empirical fits to the data and are shown in Fig. 4(c). The opening of the gap is observed at 48.3 K, in perfect agreement with the bulk structural phase transition temperature of 48 K [19]. No hysteresis was observed within the experimental errors of $\sim$2 K. The gap opens to a full size of $\Delta_{\mathrm{LE}} =$ 10–12 meV at low temperature. It is thus of the same order of magnitude as the mean-field value for the Peierls gap of $2\Delta = 3.5kT$ (14.6 meV at 48 K), but significantly smaller than the value of $\sim$0.1 eV, reported previously from an analysis of Raman data from flux grown crystals [20].

The nested Fermi surface and the above described temperature dependence of the gap suggest that the unusual ground state of $Ca_3Ru_2O_7$ does not result from an orbital selective Mott transition, as it has been proposed for $Ca_{2-x}Sr_xRuO_4$ [7], but originates from the interaction with spin, orbital or lattice degrees of freedom and bears some resemblance to a Peierls transition. Although much of the data reported in this Letter are consistent with weak coupling theory, we found several spectroscopic signatures which point beyond a nesting driven Peierls instability. The very small Z and the coexistence of heavy, non-nested bands which become similarly gapped at 48 K with a dispersive nested band suggest a more complex picture where strong and possibly orbital dependent interactions are present. Whether the observed electronic instability is the consequence or the driving force of the simultaneous structural and magnetic phase transition remains ambiguous, as does the nature of the symmetry breaking ordering, which we propose from the observed nesting vector of $(\pi/a, \pi/b)$ and the gapping of all nested states. It is hoped that the present work stimulates neutron or x-ray diffraction studies which can give direct evidence for ordering of lattice, spin, or orbital degrees of freedom. The latter has been proposed independently from recent Raman scattering, magnetization and transport measurements [21,22].

We thank G. Wigger and J. Denlinger for helpful discussions. This work has been supported by ONR Grant No. N00014-01-1-0048. Additional support from SSRL is provided by the DOE's office of Basic Energy Science, Division of Material Science with Contract No. DE-FG03-OIER45929-A001.

[1] M. Imada, A. Fujimori, and Y. Tokura, Rev. Mod. Phys. **70**, 1039 (1998).
[2] A. P. Mackenzie and Y. Maeno, Rev. Mod. Phys. **75**, 657 (2003).
[3] A. P. Mackenzie *et al.*, Phys. Rev. Lett. **76**, 3786 (1996).
[4] R. A. Borzi *et al.*, Phys. Rev. Lett. **92**, 216403 (2004).
[5] N. J. C. Ingle *et al.*, Phys. Rev. B **72**, 205114 (2005).
[6] A. Damascelli *et al.*, Phys. Rev. Lett. **85**, 5194 (2000).
[7] V. I. Anisimov *et al.*, Eur. Phys. J. B **25**, 191 (2002).
[8] S. Nakatsuji and Y. Maeno, Phys. Rev. Lett. **84**, 2666 (2000).
[9] Y. Yoshida *et al.*, Phys. Rev. B **72**, 054412 (2005).
[10] Y. Yoshida *et al.*, Phys. Rev. B **69**, 220411(R) (2004).
[11] E. Ohmichi *et al.*, Phys. Rev. B **70**, 104414 (2004).
[12] N. Kikugawa *et al.* (unpublished).
[13] Data taken at various photon energies between 16 and 41 eV showed a similarly low weight of the coherent QP.
[14] D. J. Singh and S. Auluck, Phys. Rev. Lett. **96**, 097203 (2006).
[15] D. J. Singh and I. I. Mazin, Phys. Rev. B **63**, 165101 (2001).
[16] A. V. Puchkov *et al.*, Phys. Rev. Lett. **81**, 2747 (1998).
[17] A. V. Puchkov, Z. X. Shen, and G. Cao, Phys. Rev. B **58**, 6671 (1998).
[18] J. Voit *et al.*, Science **290**, 501 (2000).
[19] The given temperatures may contain an absolute error of about 2 K at temperatures around 48 K, due to the unknown gradient within sample and sample holder.
[20] H. L. Liu *et al.*, Phys. Rev. B **60**, R6980 (1999).
[21] J. F. Karpus *et al.*, Phys. Rev. Lett. **93**, 167205 (2004).
[22] G. Cao *et al.*, New J. Phys. **6**, 159 (2004).